Balancing in Dynamic, Unstable Environments without Direct Feedback of Environment Information

Umashankar Nagarajan and Katsu Yamane

***Abstract*—This paper studies the balancing of simple planar bipedal robot models in dynamic, unstable environments like seesaw, bongoboard and board on a curved floor. This paper derives output feedback controllers that successfully stabilize seesaw, bongoboard and curved floor models using only global robot information and without any direct feedback of the dynamic environment, and hence demonstrates that direct feedback of environment information is not essential for successfully stabilizing the models considered in this paper. This paper presents an optimization to derive stabilizing output feedback controllers that are robust to disturbances on the board. It analyzes the robustness of the derived output feedback controllers to disturbances and parameter uncertainties, and compares their performance with similarly derived robust linear quadratic regulator (LQR) controllers. This paper also presents nonlinear simulation results of the output feedback controllers' successful stabilization of bongoboard, seesaw and curved floor models.**

I. Introduction

Balancing and postural stabilization is one of the most widely researched topics in bipedal robotics [1], [2], [3]. Unlike balancing in the sagittal (frontal) plane, where bipedal robots can exploit their legs' passive dynamics [4], [5], significant active control is essential to stabilize their motions in the coronal (lateral) plane [6]. Several balancing control strategies for stabilizing the unstable dynamics of 3D passive dynamic walkers in their coronal planes were presented in [7]. The balance recovery strategies of humans balancing on slacklines were studied in [8]. In [9], humans balancing on tightropes and slacklines were modeled as cart-poles balancing on circular tracks, and several balancing controllers for these simplified models were derived.

Momentum based control strategies that successfully stabilize humanoid robots on non-level, rocking floors were presented in [10], [11]. They directly determined center of pressure and ground reaction forces at each support foot to achieve the desired momenta. They, however, did not deal with unstable environments like seesaw or bongoboard. Controllers that enable planar bipedal robots to walk on a rolling cylinder were presented in [12], [13]. Approximate value function based control approaches to stabilize humanoid robots on bongoboards were presented in [14], while adaptive policy-mixing control strategies for stabilizing humanoid robots on a seesaw were presented in [15]. However, all these approaches used the environment information directly for feedback control.

This paper studies the balancing of simple planar bipedal robot models, modeled as four-bar linkages, in dynamic, unstable environments like seesaw, bongoboard and board on a curved floor as shown in Fig. 1. This paper derives output feedback controllers that successfully stabilize the seesaw, bongoboard and curved floor models using only global robot information and without any direct feedback of the dynamic environment, and hence demonstrates that direct feedback of environment information is not essential for successfully stabilizing the models considered in this paper (see Sec. IV). This paper also presents an optimization to derive output feedback controllers that maximize their robustness to disturbances, and analyzes and the robustness and performance of the derived controllers with similarly derived robust LQR controllers (see Sec. V).

U. Nagarajan is with Honda Research Institute USA Inc., Moutain View, CA 94043, USA. This work was done when he was at Disney Research, Pittsburgh, PA 15213, USA unagarajan@hra.com. K. Yamane is with Disney Research Pittsburgh, PA 15213, USA kyamane@disneyresearch.com

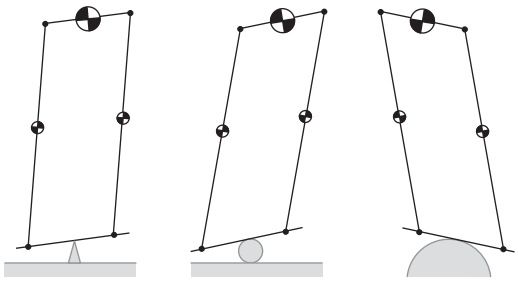

(*a*) (*b*) (*c*)

Fig. 1: Balancing in different dynamic, unstable environments: (*a*) Seesaw, (*b*) Bongoboard, and (*c*) Board on a curved floor.

II. Background: Static Output Feedback Control

A detailed survey of static output feedback control [16], [17] can be found in [18]. This section briefly describes the convergent iterative algorithm in [19] used in this paper for designing static output feedback controllers, and more details can be found in [19].

Consider a continuous time-invariant linear system

$$\begin{aligned} \dot{x} &= Ax + Bu, \\ y &= Cx, \end{aligned} \tag{1}$$

where $x \in \mathbb{R}^{n\times 1}$ is the state vector, $u \in \mathbb{R}^{m\times 1}$ is the control input vector, and $y \in \mathbb{R}^{p\times 1}$ is the output vector with $p < n$ and rank(C) = p. Without any loss of generality, the equilibrium state is given by $x = 0$. The goal of static output feedback control is to find a time-invariant output feedback gain matrix $F \in \mathbb{R}^{m\times p}$ such that $u = -Fy$ stabilizes the system in Eq. 1.

Given an output feedback gain matrix $F \in \mathbb{R}^{m\times p}$, its resulting state feedback gain matrix is given by $K = FC \in \mathbb{R}^{m\times n}$. Alternatively, given a state feedback gain matrix $K \in \mathbb{R}^{m\times n}$ that stabilizes the system in Eq. 1, the corresponding output feedback controller can be derived as

$$F = KC^{\dagger}, \tag{2}$$

where $C^{\dagger} \in \mathbb{R}^{n\times p}$ is the Moore-Penrose pseudoinverse of the output matrix $C \in \mathbb{R}^{p\times n}$. It is important to note that not all stabilizing state feedback gains K result in stabilizing output feedback gains F given by Eq. 2.

A stabilizing output feedback gain matrix F in Eq. 2 results in a stable closed-loop system $A - BFC$. The singular value decomposition of the output matrix C gives $C = USV^T$, where $S \in \mathbb{R}^{p\times n}$ is a rectangular diagonal matrix containing the singular values of C, and $U \in \mathbb{R}^{p\times p}$, $V \in \mathbb{R}^{n\times n}$ are unitary matrices, *i.e.*, $U^TU = UU^T = I_p$ and $V^TV = VV^T = I_n$. Moreover, $V = \begin{bmatrix} V_1 & V_2 \end{bmatrix}$, where $V_1 \in \mathbb{R}^{n\times p}$ and $V_2 \in \mathbb{R}^{n\times(n-p)}$. Using this, one gets

$$\begin{aligned} A - BFC &= A - BKC^{\dagger}C \\ &= A - BKVS^{\dagger}U^TUSV^T \\ &= V(V^TAV - V^TBKVS^{\dagger}S)V^T \\ &= V\left(\hat{A} - \hat{B}\begin{bmatrix} \hat{K}_1 & \hat{K}_2 \end{bmatrix}\begin{bmatrix} I_p & 0 \\ 0 & 0 \end{bmatrix}\right)V^T, \end{aligned} \tag{3}$$

where, $\hat{A} = V^TAV$, $\hat{B} = V^TB$, $\hat{K}_1 = KV_1$, $\hat{K}_2 = KV_2$, and $I_p \in \mathbb{R}^{p\times p}$ is the identity matrix. In order to avoid the loss of $\hat{K}_2$ in Eq. 3, one needs to impose the constraint $\hat{K}_2 = 0$, *i.e.*, $KV_2 = 0 \in \mathbb{R}^{m\times(n-p)}$.

The static output feedback stabilization problem can now be formulated as the following constrained optimization problem of finding a state feedback gain K:

$$\begin{aligned} \underset{K}{\text{minimize}} \quad & E\left[\int_0^\infty \left(x^T Q x + u^T R u\right) dt\right], \\ \text{subject to} \quad & KV_2 = 0, \\ & Q \geq 0,\ R > 0, \end{aligned} \tag{4}$$

where, $E[\cdot]$ is the expected value, $u = -Kx$, and $Q \in \mathbb{R}^{n\times n}$ and $R \in \mathbb{R}^{m\times m}$ are positive-semidefinite and positive-definite matrices respectively. The optimal stabilizing state feedback gain K satisfying the constraint $KV_2 = 0$ will result in an optimal stabilizing output feedback gain F given by Eq. 2.

The optimization problem in Eq. 4 is similar to that of a Linear Quadratic Gaussian (LQG) optimal control [20] problem, which is a combination of a Linear Quadratic Estimator (LQE) and a Linear Quadratic Regulator (LQR). However in contrast to LQG, Eq. 4 is a constrained optimization problem with constraints on the structure of the state feedback gain K. A problem formulation similar to that of LQG is chosen because the system in Eq. 1 has fewer outputs than the states, and hence a state estimator is essential for implementing full state feedback control. In order to solve Eq. 4, an initial posteriori estimate of the error covariance is required and it is given by

$$X = E[x(0)x(0)^T] > 0, \tag{5}$$

where $E[\cdot]$ is the expected value and $X \in \mathbb{R}^{n\times n}$ is a symmetric, positive definite matrix. More details on the LQG problem and its solution can be found in [20].

Algorithm 1 presents the iterative convergent algorithm described in [19] that solves the constrained optimization problem in Eq. 4. The matrices Q, R in Eq. 4 and X in Eq. 5 are defined by the user. The algorithm solves the algebraic Riccati equation in Eq. 6 to get the initial stabilizing state feedback gain K_0 (Step 3) for the system in Eq. 1. At every iteration i, the algorithm solves Lyapunov equations in Eq. 8−9, and uses Eq. 10 (Step 7) to update the state feedback gain such that K_{i+1} in Eq. 11 stabilizes the system in Eq. 1 and $K_{i+1}V_2 \to 0$ as $i \to \infty$. The algorithm iterates until $||K_{i+1}V_2|| < \epsilon$ (Step 5), and the norm can be either L_2-norm or Frobenius norm. Intuitively, at each iteration i, Algorithm 1 finds a state feedback gain K_i that stabilizes the system in Eq. 1, and as $i \to \infty$, it asymptotically tends to impose the constraint of $K_iV_2 = 0$ so that the corresponding output feedback gain F_i from Eq. 2 stabilizes the system in Eq. 1.

For all results presented in this paper, the Frobenius norm is used and ϵ is chosen to be 10^{-5}. The proof of convergence of Algorithm 1 and the bounds on β_i that guarantee the stability of the closed loop system (Step 8) can be found in [19]. However, in our implementation, the parameter β_i in Step 8 starts with a value of 0.1 for each iteration, and is reduced by factors of 10 if the resulting closed-loop system is unstable. This is computationally cheap and allows Algorithm 1 to converge faster.

Algorithm 1: Output Feedback Control Design

input : Linear State Space Matrices $\{A, B, C\}$
User-defined Matrices Q, R, X
output : Output Feedback Control Gain F
function: F = OutputFeedback(A, B, C, Q, R, X)

1 **begin**
2 Do singular value decomposition of C and obtain V_2
$[U, S, V]$ = svd(C)
$V_2 = V(:, p+1 : n)$
3 Solve algebraic Riccati equation for N and obtain the initial stabilizing state feedback gain K_0
$A^T N + NA - NBR^{-1}B^T N + Q = 0$ (6)
$K_0 = B^T N$ (7)
4 $i = 0$
5 **while** $||K_iV_2|| \geq \epsilon$ **do**
6 To get Y_i and P_i, solve the following Lyapunov equations
$(A - BK_i)Y_i + Y_i(A - BK_i)^T + X = 0$ (8)
$(A - BK_i)^T P_i + P_i(A - BK_i) + K_i^T R K_i + Q = 0$ (9)
7 Get the gain increment
$K_i' = R^{-1}B^T P\left[I - V_2\left(V_2^T Y^{-1} V_2\right)^{-1} V_2^T Y^{-1}\right]$ (10)
8 Update the gain
$K_{i+1} = K_i + \beta_i(K_i' - K_i)$, (11)
such that $\beta_i > 0$ and $A - BK_{i+1}$ is stable
9 $i = i + 1$
10 **end**
11 Get the output feedback gain $F = K_iC^\dagger$ (Eq. 2)
12 **end**

III. Dynamic Robot Models

Since the tasks of interest in this work are predominantly lateral balancing tasks, the planar bipedal robot model used in this paper is limited to the coronal plane of a bipedal robot and is modeled as a four-bar linkage with two position constraints and one angular constraint at the pelvis. This robot model has one degree of freedom (DOF) and four actuators corresponding to ankle and hip joints.

A. Bongoboard Model

The bongoboard is modeled as a rigid rectangular board with rolling contact on top of a rigid cylindrical wheel. The board is assumed to have negligible thickness. The bongoboard model is derived with the following assumptions: (i) the robot's feet are rigidly attached to the board and cannot slide or lose contact, (ii) there is no slip between the wheel and the board, or the wheel and the floor. For all simulation results presented in this work, the event of the board hitting the floor is ignored. The overall bongoboard model has 3-DOF, one for the planar bipedal robot and two for the bongoboard.

The bongoboard model represents a parallel system rigidly attached at its feet and constrained at its pelvis. The left and right legs are individually modeled as two links (link-1 and link-2) that are rigidly attached to the board at their respective feet, and their end-points are constrained at the pelvis with two position constraints and one

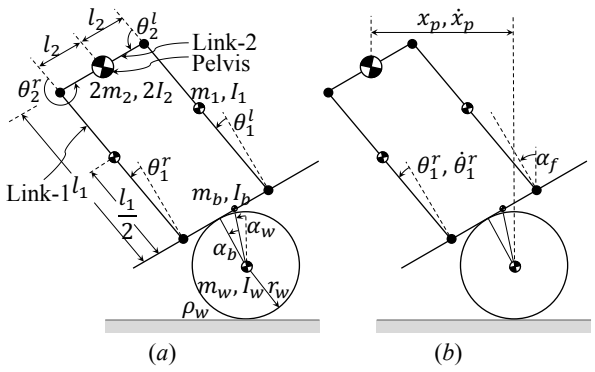

Fig. 2: Bongoboard dynamic model: (a) With its configurations and system parameters marked; and (b) With its five outputs used for output feedback control marked.

TABLE I: Nominal System Parameters for the Bongoboard Model

Parameter	Symbol	Value
Wheel Density	ρ_w	200 kg·m^{-3}
Wheel Radius	r_w	0.1 m
Wheel Mass	m_w	6.28 kg
Wheel Moment of Inertia	I_w	0.035 kg·m^2
Board Mass	m_b	2 kg
Board Moment of Inertia	I_b	0.1067 kg·m^2
Board Length	l_b	0.8 m
Link-1 Mass	m_1	15 kg
Link-1 Moment of Inertia	I_1	1 kg·m^2
Link-1 Length	l_1	1 m
Link-2 Half Mass	m_2	15 kg
Link-2 Half Moment of Inertia	I_2	2 kg·m^2
Link-2 Half Length	l_2	0.1 m

angular constraint. Figure 2(a) shows the bongoboard model along with its configurations, and the nominal system parameters are listed in Table I. The configuration vector of the bongoboard model is given by $q = [\alpha_w, \alpha_b, \theta_1^l, \theta_1^r, \theta_2^l, \theta_2^r]^T \in \mathbb{R}^{6\times1}$, where α_w is the configuration of the wheel/cylinder, α_b is the configuration of the board relative to the wheel, θ_1^l, θ_1^r are the link-1 configurations of the left and right legs respectively relative to the board, and θ_2^l, θ_2^r are the link-2 configurations of the left and right legs respectively relative to their first links.

The equations of motion are derived using Euler-Lagrange equations and can be written in matrix form as follows:

$$M(q)\ddot{q} + c(q,\dot{q}) + g(q) = s_\tau^T\tau + \Psi(q)^T\lambda, \tag{12}$$

where $M(q) \in \mathbb{R}^{6\times6}$ is the mass/inertia matrix, $c(q,\dot{q}) \in \mathbb{R}^{6\times1}$ is the vector of Coriolis and centrifugal forces, $g(q) \in \mathbb{R}^{6\times1}$ is the vector of gravitational forces, $s_\tau = \begin{bmatrix} 0_{4\times2} & I_4 \end{bmatrix} \in \mathbb{R}^{4\times6}$ is the input coupling matrix, $I_4 \in \mathbb{R}^{4\times4}$ is the identity matrix, $\tau \in \mathbb{R}^{4\times1}$ is the vector of actuator inputs, $\Psi(q) \in \mathbb{R}^{3\times6}$ is the constraint matrix, and $\lambda \in \mathbb{R}^{3\times1}$ is the vector of Lagrange multipliers. The system matrices in Eq. 12 have long symbolic expressions, and hence are not presented here. The constraints given by $\Psi(q)\dot{q} = 0 \in \mathbb{R}^{3\times1}$ are differentiated to get

$$\Psi(q)\ddot{q} + \dot{\Psi}(q,\dot{q})\dot{q} = 0 \in \mathbb{R}^{3\times1}. \tag{13}$$

In Eq. 12, $\lambda \in \mathbb{R}^{3\times1}$ represents the vector of constraint forces at the pelvis corresponding to the two position constraints and one angular constraint, and does not represent the contact forces at the feet. In this model, the contact forces at the feet are ignored since the feet are assumed to be rigidly fixed to the board. For an actual bipedal robot, this can be achieved by strapping the robot to the board like in a snowboard.

Since the mass/inertia matrix $M(q)$ is always a symmetric, positive-definite matrix, it is always invertible. Therefore, from Eq. 12,

$$\ddot{q} = M^{-1}(q)(s_\tau^T\tau - c(q,\dot{q}) - g(q)) + M^{-1}(q)\Psi(q)^T\lambda. \tag{14}$$

Solving for λ from Eq. 13 and Eq. 14,

$$\lambda = -\Psi^{T\#}(q)s_\tau^T\tau - \mu(q,\dot{q}) - \eta(q), \tag{15}$$

where,

$$\begin{aligned}
M_\Psi(q) &= (\Psi(q)M^{-1}(q)\Psi(q)^T)^{-1}, &(16)\\
\Psi^{T\#}(q) &= M_\Psi(q)\Psi(q)M^{-1}(q), &(17)\\
\mu(q,\dot{q}) &= M_\Psi(q)\Big(\dot{\Psi}(q,\dot{q})\dot{q} - \Psi(q)M^{-1}(q)c(q,\dot{q})\Big), &(18)\\
\eta(q) &= M_\Psi(q)\Psi(q)M^{-1}(q)g(q), &(19)
\end{aligned}$$

where $M_\Psi(q)$ is known as the operational space inertia matrix [21], and $\Psi^{T\#}$ is the generalized inverse of Ψ^T weighted by M^{-1}.

Combining Eq. 14 and Eq. 15, $\ddot{q}$ can be written as

$$\begin{aligned}
\ddot{q} &= M^{-1}(q)\Big[N_\Psi(q)s_\tau^T\tau - c(q,\dot{q}) - g(q) - h(q,\dot{q})\Big],\\
&= \Phi(q,\dot{q},\tau), &(20)
\end{aligned}$$

where,

$$\begin{aligned}
N_\Psi(q) &= I_6 - \Psi^T(q)\Psi^{T\#}(q), &(21)\\
h(q,\dot{q}) &= \Psi^T(q)(\mu(q,\dot{q}) + \eta(q)), &(22)
\end{aligned}$$

where $I_6 \in \mathbb{R}^{6\times6}$ is the identity matrix. The above derivation (Eq. 12−22) is similar to the one presented in [22].

The linear state space matrices corresponding to the state vector $x = [q^T, \dot{q}^T]^T \in \mathbb{R}^{12\times1}$ are:

$$\begin{aligned}
A &= \begin{bmatrix} 0_{6\times6} & I_6 \\ \frac{\partial\Phi(q,\dot{q},\tau)}{\partial q} & \frac{\partial\Phi(q,\dot{q},\tau)}{\partial\dot{q}} \end{bmatrix}\Bigg|_{x=0,\tau=0} \in \mathbb{R}^{12\times12},\\
B &= \begin{bmatrix} 0_{6\times4} \\ \frac{\partial\Phi(q,\dot{q},\tau)}{\partial\tau} \end{bmatrix}\Bigg|_{x=0,\tau=0} \in \mathbb{R}^{12\times4}. &(23)
\end{aligned}$$

The constraints in Eq. 13 reduce the degrees of freedom of the system and hence make the pair (A, B) in Eq. 23 not controllable. Given an output matrix $C \in \mathbb{R}^{p\times12}$, where rank($C$) = p, the state space realization $\{A, B, C\}$ can be converted into its minimal (controllable and observable) realization $\{A_m, B_m, C_m\}$ using Kalman decomposition [23], which provides an orthonormal state transformation matrix $U_m \in \mathbb{R}^{6\times12}$ such that

$$\begin{aligned}
A_m &= U_m A U_m^T \in \mathbb{R}^{6\times6},\\
B_m &= U_m B \in \mathbb{R}^{6\times4},\\
C_m &= C U_m^T \in \mathbb{R}^{p\times6}. &(24)
\end{aligned}$$

The original realization of the bongoboard model in Eq. 23 with twelve states is reduced to its minimal realization in Eq. 24 with only six states, wherein six states corresponding to the three (two position and one rotational) constraints in Eq. 13 have been removed.

B. Seesaw and Curved Floor Models

The model of the planar bipedal robot on a seesaw and on a board on top of a curved floor as shown in Fig. 1(b)−(c) have only 2-DOF, one each for the planar bipedal robot and the board. Therefore, the minimal system has only four states. These models can be derived similar to the bongoboard model presented in Sec. III-A, wherein the wheel configuration α_w is omitted. However, for the seesaw model, the board is attached to the floor at its center via a hinge joint, whereas, for the curved floor model, the board has a rolling contact on a rigid semicylinder. Just like the bongoboard model, both these models assume that the robot's feet are rigidly attached to the board, and hence do not slide or lose contact.

IV. Balancing without Direct Feedback of Environment Information

This section demonstrates that direct feedback of environment information is not essential for successfully stabilizing bongoboard, seesaw and curved floor models presented in Sec. III. The environment information for the bongoboard model consist of the wheel angle α_w and the board angle α_b relative to the wheel, while that for the seesaw and curved floor models consists of only the board angle α_b.

A. Bongoboard Model

Algorithm 1 requires the number of outputs to be fewer than the number of states, *i.e.*, $p < n$, and the output matrix $C \in \mathbb{R}^{p\times n}$ must be of full row rank, *i.e.*, rank(C) = p. Therefore, for the bongoboard model with six minimal states, one can pick a maximum of five outputs. Here, the output vector $y \in \mathbb{R}^{5\times 1}$ is chosen as

$$y = \begin{bmatrix} x_p & \dot{x}_p & \theta_1^r & \dot{\theta}_1^r & \alpha_f \end{bmatrix}^T, \tag{25}$$

where $x_p, \dot{x}_p$ are the global position and velocity of the pelvis respectively, $\theta_1^r, \dot{\theta}_1^r$ are the angle and angular velocity of the right link-1 respectively, and α_f is the global foot angle as shown in Fig. 2(b).

The global foot angle α_f and global position and velocity of the pelvis $(x_p, \dot{x}_p)$ can be estimated using an inertial measurement unit [24], [25] at the pelvis. It is important to note that these outputs can be measured or estimated without using direct measurements of the environment, *i.e.*, wheel angle α_w and board angle α_b relative to the wheel. The corresponding output matrix $C \in \mathbb{R}^{5\times 12}$ can be used in Eq. 24 to derive the minimal system $\{A_m, B_m, C_m\}$ with $C_m \in \mathbb{R}^{5\times 6}$.

If there exists a set of Q, R (Eq. 4) and X (Eq. 5) matrices for which Algorithm 1 finds a stabilizing output feedback controller for the minimal bongoboard model with the five outputs in Eq. 25 that do not directly use the environment information, then this shows that direct feedback of environment information is not essential for stabilizing the bongoboard model in Sec. III-A.

In fact, with identity matrices chosen for R and X, there exists a large family of Q matrices for which stabilizing output feedback controllers can be derived for the bongoboard model in Sec. III-A. Section V presents an algorithm that finds a Q matrix such that the resulting closed-loop system with output feedback is robust to disturbances. For one such Q matrix, Fig. 3(a) shows semi-logarithmic plots of the Frobenius norm $||KV_2||_F$ with increasing iterations of Algorithm 1 for the bongoboard model with five, four and three outputs. Figure 3(a) demonstrates that the first three outputs in Eq. 25, *i.e.*, $[x_p, \dot{x}_p, \theta_1^r]$, are sufficient to design stabilizing output feedback controllers for the bongoboard model.

B. Seesaw and Curved Floor Models

Since both seesaw and curved floor models have four minimal states, one can use a maximum of three outputs for the output feedback control design. Here, the output vector $y \in \mathbb{R}^{3\times 1}$ is chosen as

$$y = \begin{bmatrix} x_p & \dot{x}_p & \theta_1^r \end{bmatrix}^T, \tag{26}$$

where $x_p, \dot{x}_p$ are the global position and velocity of the pelvis respectively, and θ_1^r is the right link-1 angle as shown in Fig. 2(b). These three outputs match the first three outputs in Eq. 25, and are not obtained using any direct measurement of the environment, *i.e.*, board angle α_b. Figure 3(b) shows semi-logarithmic plots of the Frobenius norm $||KV_2||_F$ with increasing iterations of Algorithm 1 for seesaw and curved floor models.

Figure 3 shows that the three outputs in Eq. 26 that do not include direct environment information are sufficient to successfully stabilize the bongoboard, seesaw and curved floor models considered in this paper. This shows that direct feedback of environment information is not essential for balancing in dynamic, unstable environments considered in this paper.

It is to be noted that although the output feedback controllers with three outputs (Eq. 26) derived in this paper for the bongoboard, seesaw and curved floor models feedback the same outputs, the controllers are different from each other and are derived using their respective models. However, it is actually possible to design a single output feedback controller that can stabilize all the three models with the same outputs, and a detailed description of such a control design is presented in [26]. In this paper, we restrict our study to demonstrating that dynamic, unstable systems like the bongoboard, seesaw and curved floor models in Fig. 1 can be stabilized without direct feedback of environment information.

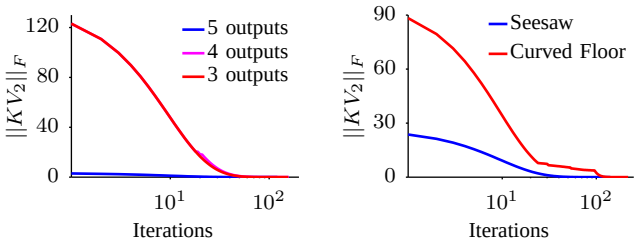

Fig. 3: Semi-logarithmic plots of the Frobenius norm $||KV_2||_F$ converging to zero producing stabilizing output feedback controllers using Algorithm 1: (a) Bongoboard model with different number of outputs, and (b) Seesaw and curved floor models with three outputs.

V. Robust Output Feedback Control Design

Section IV demonstrated that Algorithm 1 can be used to derive output feedback controllers that successfully stabilize the bongoboard, seesaw and curved floor models without direct feedback of environment information. Since disturbance rejection is a key feature of any stabilizing controller, this section focuses on deriving stabilizing output feedback controllers that are robust to disturbances on the board. The presented approach, however, is not limited to disturbances on the board and can include other disturbances as well.

Given the user defined matrices Q, R (Eq. 4) and X (Eq. 5), Algorithm 1 derives a stabilizing output feedback controller. For all results presented in this paper, the matrices R, X are chosen to be identity matrices. Therefore, in this case, the only free, tunable parameter in Algorithm 1 is the state gain matrix $Q \in \mathbb{R}^{n\times n}$. This section formulates the robust output feedback controller design problem as a problem of finding the Q matrix in Eq. 4 such that the resulting closed loop system with output feedback is robust to disturbances on the board.

A. Disturbance H_∞ norm

Given the system $\{A, B, C\}$ in Eq. 1 and a stabilizing output feedback gain $F \in \mathbb{R}^{m\times p}$, the linear state space matrices of the closed loop system used for disturbance rejection analysis are:

$$\begin{aligned} A^d &= A - BFC \in \mathbb{R}^{n\times n}, \\ B^d &= \begin{bmatrix} 0 \\ M^{-1}(q)N_\Psi(q)s_d^T \end{bmatrix}\Big|_{q=0} \in \mathbb{R}^{n\times 1}, \\ C^d &= I \in \mathbb{R}^{n\times n}, \end{aligned} \tag{27}$$

where q is the vector of generalized coordinates, $M(q)$ is the mass/inertia matrix, $N_\Psi(q)$ is of the form shown in Eq. 21, and s_d is the disturbance transfer matrix, and is similar to the input coupling matrix s_τ in Eq. 12. The disturbance torque on the board is the input to the system in Eq. 27, and all states are chosen as the outputs. Just like in Eq. 20, s_d^T maps the input (disturbance torque on the board) to a vector of generalized forces, and $M^{-1}(q)N_\Psi(q)$ maps the resulting vector of generalized forces to a vector of generalized accelerations. Since we are interested only in disturbances on the board, the disturbance transfer matrix is chosen to be $s_d = [0, 1, 0, 0, 0, 0] \in \mathbb{R}^{1\times 6}$

for the bongoboard model and $s_d = [1, 0, 0, 0, 0] \in \mathbb{R}^{1\times 5}$ for the seesaw and curved floor models.

Using the minimal realization $\{A_m^d, B_m^d, C_m^d\}$ of the system $\{A^d, B^d, C^d\}$ in Eq. 27, the transfer function G^d from the disturbance on the board to all states can be written in matrix form as:

$$G^d = \begin{bmatrix} A_m^d & B_m^d \\ C_m^d & 0 \end{bmatrix}. \tag{28}$$

The norm $||G^d||_\infty$ represents the sensitivity of all states of the system to the disturbance on the board. Lower the norm, lower is the sensitivity and more robust is the output feedback controller to the disturbances on the board. Hence, it is desirable to reduce $||G^d||_\infty$ to design robust output feedback controllers.

B. Optimizing Robust Output Feedback Controllers

In this work, the matrix $Q \in \mathbb{R}^{12\times 12}$ for the bongoboard model in Sec. III-A is chosen to be a diagonal matrix, with equal weights for the configurations of the left and right legs. Therefore, the matrix $Q \in \mathbb{R}^{12\times 12}$ for the bongoboard model is parameterized by eight parameters as follows:

$$Q = diag\big([a_1, a_2, a_3, a_3, a_4, a_4, a_5, a_6, a_7, a_7, a_8, a_8]^T\big), \tag{29}$$

and the matrix $Q_m \in \mathbb{R}^{6\times 6}$ corresponding to the minimal system $\{A_m, B_m, C_m\}$ in Eq. 24 is obtained as $Q_m = U_m Q U_m^T$. The matrix $Q \in \mathbb{R}^{10\times 10}$ for the seesaw and curved floor models are also parametrized similarly. As mentioned earlier, the other user-defined matrices R_m and X_m corresponding to the minimal system are chosen to be identity matrices. For a given Q_m, the output feedback control gain F for the minimal system is obtained using Algorithm 1.

The robust output feedback control design is formulated as an optimization problem of finding the parameters $\{a_i\}$ of Q in Eq. 29 such that the resulting stabilizing output feedback controller minimizes the disturbance H_∞ norm of its closed loop system in Eq. 28 as follows:

$$\underset{\{a_i\}}{\text{minimize}} \quad J = ||G^d||_\infty + w||K||_\infty, \tag{30}$$

where, w is an user-defined weight, $K = FC$, F is the output feedback gain derived using Algorithm 1, and G^d is the transfer function from the disturbance torque on the board to the outputs of the closed loop system shown in Eq. 28. The term $||K||_\infty$ is used as a regularizer to avoid high gain controllers that produce large torque outputs. This can also be achieved by using $||Q||_\infty$ instead of $||K||_\infty$.

For all results presented in this paper, the weight w is chosen to be 10^{-5}, and the optimization is performed using the Nelder-Mead simplex method [27], which solves the optimization in Eq. 30 using only functional evaluations. The Nelder-Mead simplex method is chosen because the objective function J in Eq. 30 has no closed-form representation in terms of the parameters $\{a_i\}$ of Q in Eq. 29, and hence its Jacobians and Hessians cannot be computed for use with other gradient-based algorithms.

VI. Robustness Analysis and Simulation Results

This section analyzes the robustness of the robust output feedback controllers derived in Sec. V, and presents simulation results that validate their robustness and performance in stabilizing the nonlinear dynamics of bongoboard, seesaw and curved floor models. Moreover, this section compares the robustness of the robust output feedback controllers to disturbances and modeling uncertainties with that of similarly derived robust linear quadratic regulators (LQR). The Q matrices for the LQR controllers with full state feedback are obtained using an optimization similar to Eq. 30, and hence the LQR controllers are also robust to disturbances on the board. The constrained nonlinear dynamics of the seesaw, curved floor and bongoboard models are simulated in MATLAB using ode15s, and the actuator torques are limited to ± 200 Nm. Moreover, the joint angle limits are set to $\pm 50^\circ$. The simulation stops when the joint angles hit their limits, and it is considered as a failure.

TABLE II: Disturbance Rejection: LQR vs Output Feedback (OFC)

System	Control Design	Disturbance Rejection	
		$\|\|\mathbf{G^d}\|\|_\infty$	Max. Disturbance Torque for 0.1 s
Bongoboard	LQR	0.6313	109.8 Nm
	OFC (5 outputs)	0.6783	87.2 Nm
	OFC (4 outputs)	3.4963	57.4 Nm
	OFC (3 outputs)	3.5649	54.5 Nm
Seesaw	LQR	0.3802	73.8 Nm
	OFC (3 outputs)	0.4748	60.7 Nm
Curved Floor	LQR	0.1503	146.7 Nm
	OFC (3 outputs)	0.2109	194.8 Nm

A. Robustness to Disturbances on the Board

The disturbance rejection results of the robust LQR and output feedback controllers with different number of outputs derived using the optimization in Eq. 30 are presented in Table II. The listed disturbance H_∞ norms are calculated using Eq. 28 of the linearized system, whereas the maximum disturbance torques on the board for 0.1 s that the controllers can successfully reject are obtained from nonlinear simulations of the different models.

Table II shows that the robust LQR controllers result in a smaller $||G^d||_\infty$ and successfully reject larger disturbances than the robust output feedback controllers. It is important to note that the robust LQR controllers were also derived using an optimization similar to the one used for deriving the robust output feedback controllers (Eq. 30). In addition to being optimized for robustness to disturbances on the board, the robust LQR controllers have full state feedback and hence, perform better than the robust output feedback controllers that use fewer outputs than states. However, Table II also shows that the best performing robust output feedback controller is able to reject about 80% of the disturbance torque that the best performing robust

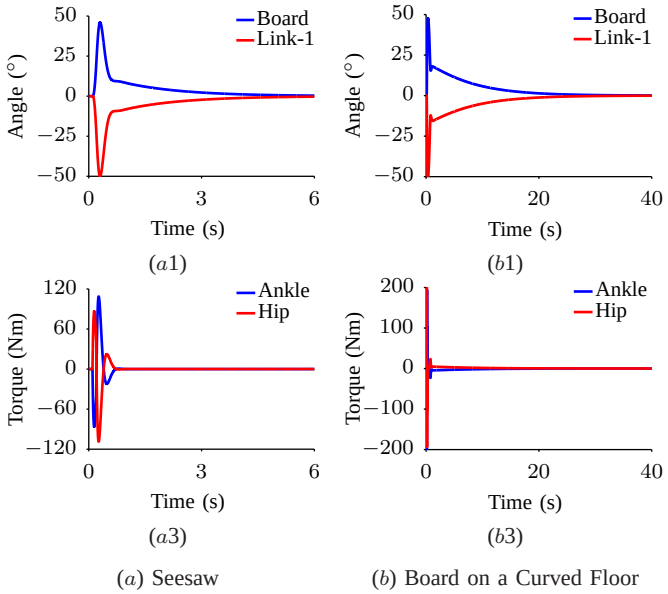

(a) Seesaw (b) Board on a Curved Floor

Fig. 4: Output feedback controllers' successful efforts in stabilizing seesaw and curved floor models with three outputs when subjected to the following disturbances for 0.1 s: (a) 60.7 Nm, and (b) 194.8 Nm.

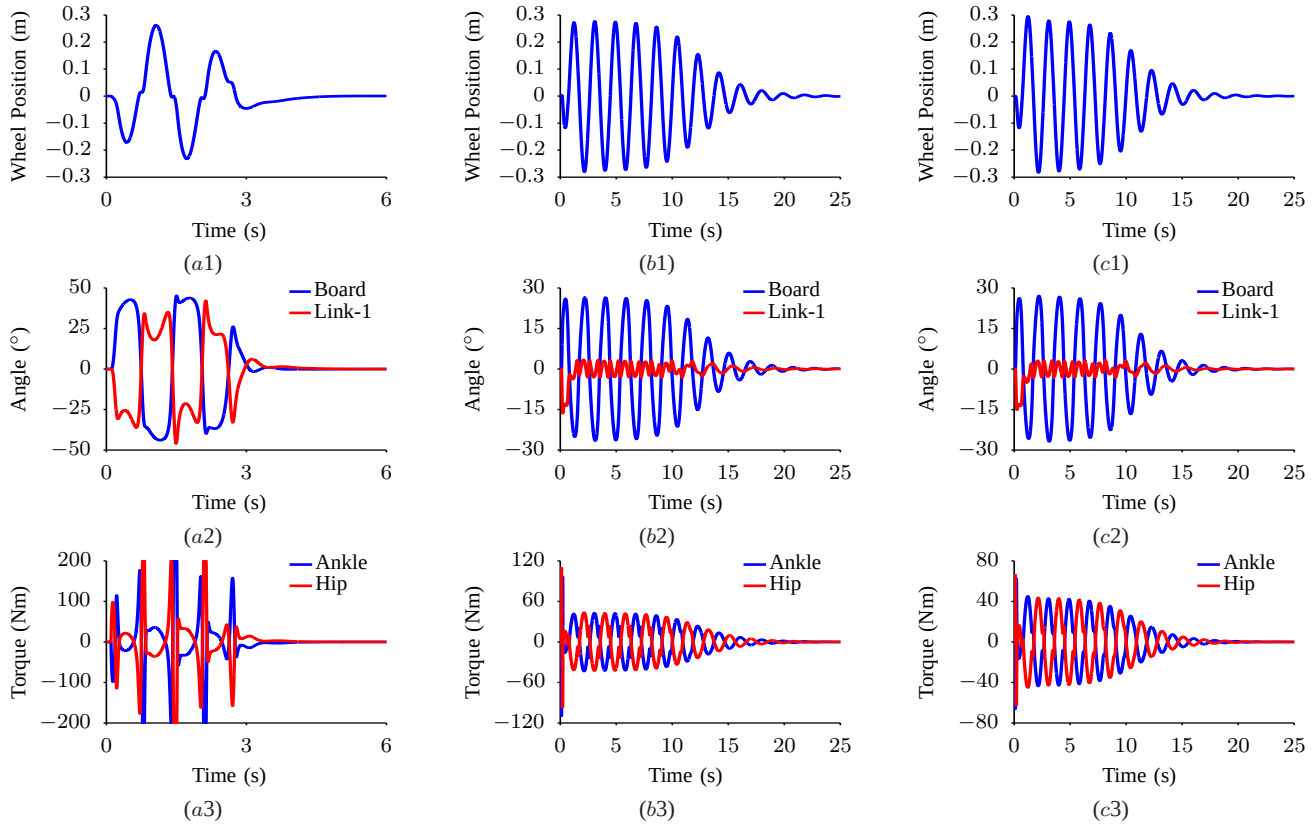

(a) Output feedback with 5 outputs (b) Output feedback with 4 outputs (c) Output feedback with 3 outputs

Fig. 5: Output feedback controllers' successful efforts in stabilizing bongoboard models when subjected to the following board disturbances for 0.1 s: (a) 87.2 Nm, (b) 57.4 Nm, and (c) 54.5 Nm.

LQR controller can reject for both bongoboard and seesaw models, whereas, for the curved floor model, the robust output feedback controller outperforms the robust LQR controller by rejecting a much larger (133%) disturbance torque on the board. This demonstrates that the output feedback controllers with no direct feedback of environment information can have comparable disturbance rejection performance with that of the LQR controllers with full state feedback.

Figures 4(a) and 4(b) present the board and link-1 angle trajectories, and also the ankle and hip torque trajectories resulting from the successful stabilization of the seesaw and curved floor models respectively using the robust output feedback controllers derived in Sec. V with three outputs. Similarly, the trajectories of the wheel position, global board angle, link-1 angle, ankle torque and hip torque for the bongoboard model stabilized by robust output feedback controllers derived in Sec. V with different number of outputs are shown in Fig. 5. The results presented in Fig. 4$-$5 correspond to the simulations wherein the seesaw, curved floor and bongoboard models are subjected to the maximum disturbance torques listed in Table II for 0.1 s. In this work, the robot model is redundantly actuated, and hence the hip and ankle torque trajectories are equal and opposite to each other. The companion video visualizes the planar bipedal robot achieving the motions shown in Fig. 4$-$5.

B. Robustness to Modeling Uncertainties

Table III presents the range of parameter uncertainties in the environment, $i.e.$, wheel and board, that the different controllers can handle. For each parameter except the wheel radius r_w and wheel density ρ_w, while the parameter is varied, the other environment parameters are maintained at their nominal values. Assuming a constant density wheel, the mass m_w and moment of inertia I_w are varied quadratically and quartically respectively with the wheel radius r_w, whereas both the values are varied linearly with the wheel density ρ_w. The lower and upper bounds of the stabilizable parameter range are calculated using a bisection algorithm that uses the linearized models. Among the values listed in Table III, a stabilizable range written as $(0, \cdot]$ refers to a range whose lower bound is $< 10^{-4}$, and similarly, a stabilizable range written as $[\cdot, \infty)$ refers to a range whose upper bound is $> 10^{6}$.

For the bongoboard model, it can be seen that the robust output feedback controller with five outputs outperforms the robust LQR controller in all environment parameters except in the moment of inertia (MOI) of the board. Particularly, the robust output feedback controller with five outputs is significantly more robust to the wheel parameters than the robust LQR controller. The robust output feedback controller for the seesaw model matches the performance of the robust LQR controller, whereas, for the curved floor model, the robust LQR controller outperforms the robust output feedback controller.

Although Table III lists the stabilizable parameter ranges for the robust output feedback controllers derived in Sec. V, it is interesting to note that the output feedback controllers, in general, have better robustness to modeling uncertainties than LQR controllers with full state feedback. Particularly, their robustness to uncertainties in the environment parameters is significantly better than that of LQR controllers with full state feedback.

VII. Conclusions

This paper derived output feedback controllers that successfully stabilize seesaw, bongoboard and curved floor models using only global robot information and without any direct feedback of the dynamic environment, and hence demonstrated that direct feedback of

TABLE III: Range of Stabilizable Environment Parameters: LQR vs Output Feedback Control (OFC)

System	Environment Parameter	Symbol	Unit	Nominal Value	Stabilizable Parameter Range			
					LQR	Output Feedback Control (OFC)		
						5 outputs	4 outputs	3 outputs
Bongoboard	Wheel Radius	r_w	m	0.1	[0.0836, 0.1039]	[0.0005, 0.4038]	[0.0624, 0.4022]	[0.0616, 9.2255]
	Wheel Density	ρ_w	kg·m^{-3}	200	(0, 8989.7827]	(0, ∞)	(0, 966.7624]	(0, 993.4203]
	Wheel Mass	m_w	kg	6.28	(0, 420.4918]	(0, ∞)	(0, 42.4161]	(0, 43.6723]
	Wheel MOI	I_w	kg·m^2	0.035	(0, 4.1734]	(0, ∞)	(0, 0.3928]	(0, 0.4054]
	Board Mass	m_b	kg	2	(0, 4.4538]	(0, 9.4737]	(0, 13.8347]	(0, 11.6275]
	Board MOI	I_b	kg·m^2	0.1067	(0, 7.9182]	(0, 4.0927]	(0, 1.6884]	(0, 1.7221]
Seesaw	Board Mass	m_b	kg	2	(0, ∞)	N/A	N/A	(0, ∞)
	Board MOI	I_b	kg·m^2	0.1067	(0, ∞)	N/A	N/A	(0, ∞)
Curved Floor	Wheel Radius	r_w	m	0.1	[0.0710, 30.5383]	N/A	N/A	[0.0840, 1.4462]
	Board Mass	m_b	kg	2	(0, 18873.7852]	N/A	N/A	(0, 836.7009]
	Board MOI	I_b	kg·m^2	0.1067	(0, ∞)	N/A	N/A	(0, ∞)

environment information is not essential for successfully stabilizing the models considered in this paper. This paper also presented an optimization to derive robust output feedback controllers and compared their performance with similarly derived robust LQR controllers. When compared to the robust LQR controllers with full state feedback, the robust output feedback controllers have comparable robustness to disturbances and significantly better robustness to modeling uncertainties. Hence, they form viable alternatives to traditional full state feedback controllers.

VIII. Future Work

As part of future work, the derived robust output feedback controllers need to be experimentally validated. In this work, the outputs needed to stabilize the system were hand-picked using the designer's intuition. Automatic approaches to determine these outputs is an interesting future direction to explore. The motion capture data of humans balancing in dynamic, unstable environments like seesaw and bongoboards can be potentially used to obtain these outputs. Given a dynamic environment, proving the existence or non-existence of a set of outputs that make the system output feedback stabilizable remains an open research problem.

This paper demonstrated that direct feedback of environment information is not essential for successfully stabilizing the simple planar bipedal models considered in this paper. However, its validity remains to be proved in general. The dynamic models considered in this paper assumed that the robot's feet were rigidly attached to the board. The models can be modified to include contact forces at the feet, and constraints on these contact forces need to be considered in the output feedback control design.

IX. Acknowledgement

The authors thank the reviewers and the associate editor for their valuable suggestions that helped improve the paper significantly.

References

[1] J. Pratt, J. Carff, S. Drakunov, and A. Goswami, "Capture point: A step toward humanoid push recovery," in *Proc. IEEE-RAS Int'l Conf. on Humanoid Robots*, 2006, pp. 200–207.

[2] B. Stephens, "Humanoid push recovery," in *Proc. IEEE Int'l Conf. on Humanoid Robots*, 2007, pp. 589–595.

[3] C. Ott, M. A. Roa, and G. Hirzinger, "Posture and balance control for biped robots based on contact force optimization," in *Proc. IEEE Int'l Conf. on Humanoid Robots*, 2011, pp. 26–33.

[4] T. McGeer, "Passive dynamic walking," *Int'l Journal of Robotics Research*, vol. 9, no. 2, pp. 62–82, 1990.

[5] S. H. Collins, M. Wisse, and A. Ruina, "A three-dimensional passive-dynamic walking robot with two legs and knees," *Int'l Journal of Robotics Research*, vol. 20, no. 7, pp. 607–615, 2001.

[6] C. E. Bauby and A. D. Kuo, "Active control of lateral balance in human walking," *Journal of Biomechanics*, vol. 33, no. 11, pp. 1433–1440, 2000.

[7] A. D. Kuo, "Stabilization of lateral motion in passive dynamic walking," *Int'l Journal of Robotics Research*, vol. 18, no. 9, pp. 917–930, 1999.

[8] P. Huber and R. Kleindl, "A case study on balance recovery in slacklining," in *Proc. Int'l Conf. on Biomechanics in Sports*, 2010.

[9] P. Paoletti and L. Mahadevan, "Balancing on tightropes and slacklines," *J. R. Soc. Interface*, vol. 9, no. 74, pp. 2097–2108, 2012.

[10] S.-H. Lee and A. Goswami, "Ground reaction force control at each foot: A momentum-based humanoid balance controller for non-level and non-stationary ground," in *Proc. IEEE/RSJ Int'l Conf. on Intelligent Robots and Systems*, 2010, pp. 3157–3162.

[11] ——, "A momentum-based balance controller for humanoid robots on non-level and non-stationary ground," *Autonomous Robots*, vol. 33, no. 4, pp. 399–414, 2012.

[12] Y. Zheng and K. Yamane, "Ball walker: a case study of humanoid robot locomotion in non-stationary environments," in *Proc. IEEE Int'l Conf. on Robotics and Automation*, 2011, pp. 2021–2028.

[13] ——, "Optimization and control of cyclic biped locomotion on a rolling ball," in *Proc. IEEE Int'l Conf. on Humanoid Robots*, 2011, pp. 752–759.

[14] S. O. Anderson, J. K. Hodgins, and C. G. Atkeson, "Approximate policy transfer applied to simulated bongo board balance," in *Proc. IEEE Int'l Conf. on Humanoid Robots*, 2007, pp. 490–495.

[15] S. O. Anderson and J. K. Hodgins, "Adaptive torque-based control of a humanoid robot on an unstable platform," in *Proc. IEEE Int'l Conf. on Humanoid Robots*, 2010, pp. 511–517.

[16] A. Trofino-Neto, "Stabilization via static output feedback," *IEEE Trans. on Automatic Control*, vol. 38, no. 5, pp. 764–765, 1993.

[17] A. A. Pimpalkhare and B. Bandyopadhyay, "Comments on "stabilization via static output feedback"," *IEEE Trans. on Automatic Control*, vol. 39, no. 5, p. 1148, 1994.

[18] V. L. Syrmos, C. T. Abdallah, P. Dorato, and K. Grigoriadis, "Static output feedback - a survey," *Automatica*, vol. 33, no. 2, pp. 125–137, 1997.

[19] J. Yu, "A convergent algorithm for computing stabilizing static output feedback gains," *IEEE Trans. on Automatic Control*, vol. 49, no. 12, pp. 2271–2275, 2004.

[20] R. Stengel, *Optimal Control and Estimation*. Dover Publications, 1994.

[21] O. Khatib, "A unified approach to motion and force control of robot manipulators: The operational space formulation," *IEEE Journal of Robotics and Automation*, vol. 3, no. 1, pp. 43–53, 1987.

[22] J. Park and O. Khatib, "Contact consistent control framework for humanoid robots," in *Proc. IEEE Int'l Conf. on Robotics and Automation*, 2006, pp. 1963–1969.

[23] M. M. Rosenbrock, *State-Space and Multivariable Theory*. John Wiley, 1970.

[24] Y.-L. Tsai, T.-T. Hu, H. Bae, and P. Chou, "EcoIMU: A dual triaxial-accelerometer inertial measurement unit for wearable applications," in *Proc. Int'l Conf. on Body Sensor Networks*, 2010.

[25] J. Kelly and G. S. Sukhatme, "Fast relative pose calibration for visual and inertial sensors," in *Proc. Int'l Symp. Experimental Robotics*, 2008.

[26] U. Nagarajan and K. Yamane, "Universal balancing controller for robust lateral stabilization of bipedal robots in dynamic, unstable environments," *IEEE Int'l Conf. on Robotics and Automation (To Appear)*, 2014.

[27] J. Nelder and R. Mead, "A simplex method for function minimization," *The Computer Journal*, vol. 7, pp. 308–313, 1964.